# 8B.4 A Cyclic Tornadic Supercell on May 10, 2010: Analysis of a VORTEX2 Case

Donald W. Burgess * and Christopher M. Schwarz
Cooperative Institute for Mesoscale Meteorological Studies, The University of Oklahoma, and NOAA, NSSL, Norman, OK

Jeffery C. Snyder, Michael M. French, and Howard B. Bluestein
School of Meteorology, University of Oklahoma, Norman, OK

And Conrad L. Ziegler
NOAA, National Severe Storms Laboratory, Norman, OK

## 1. INTRODUCTION

A cyclic, tornadic supercell thunderstorm occurred on May 10, 2010; a time period during the Verification of the Origins of Rotation in Tornadoes Experiment, Part 2 (VORTEX2). The storm and its environment were sampled by two mobile X-band radars (both dual-polarized), several mobile mesonet vehicles, one mobile disdrometer vehicle, and several mobile sounding systems. The supercell formed in an environment conducive to strong supercells (large CAPE and strong vertical wind shear). Over the supercell's 6-hour lifetime, it produced at least 11 mesocyclones and 20 tornadoes. VORTEX2 radar observations covered only a small portion of the storm's path (2334 to 0000 UTC; all times are UTC).

Section 2 will discuss single-Doppler analysis from NEXRAD radars (KTLX and KINX) for the full storm life and from the NOAA (NSSL) X-band dual-Polarized radar (NOXP) for a 26-minute period. Section 3 will discuss dual-Doppler analysis for a short 8-minute interal using data from NOXP and the University of Massachusetts X-band Polarized (UMXP) radar. Section 4 will mention conclusions and discuss future work.

## 2. SINGLE-DOPPLER ANALYSIS

Utilizing techniques for recognition of vortex signatures within single-Doppler data (Burgess *et al*, 1993), the evolution of the cyclic mesocyclones are studied. Relying on the relationship of vorticity to azimuthal shear for a Rankine-combined vortex, mesocyclone vertical vorticity is estimated.

*corresponding author address: Don Burgess, NSSL/WRDD/Rm 3933, National Weather Center, 120 David L. Boren Blvd., Norman, OK 73072-7323 email: Donald.Burgess@noaa.gov

### 2.1 KTLX and KINX Data

A plot of all storm mesocyclone centers at ~1 km ARL is shown in Fig 1. The 1st mesocyclone (M1; 2215 – 2302) is associated with the tornadoes that struck east Norman and the Lake Thunderbird/Little Axe areas (EF1, EF4, and EF2). M2 (2257 – 2355) forms as M1 is occluding and produces the tornado that strikes Tecumseh and Seminole Airport (EF3). M3 (2336 – 0012) forms as M2 is occluding and produces the tornado that strikes Clearview. M4 (2359 – 0025) and succeeding mesocyclones form and produce tornadoes after the VORTEX2 analysis period ends and will not be discussed. It is interesting to note that the recurrence interval between mesocyclone formations is ~47 min for the first 3 mesocyclones (M1 – M3), becomes as short as ~17 min for M6 – M8, and returns to ~30 min for M9 – M11.

A KTLX time/height plot of single-Doppler-estimated vertical vorticity for M2 (Fig 2) reveals that the NOXP data collection region (within the dark line) captures only the weakening and dissipating stages of M2. A KTLX time/height plot of single-Doppler-estimated vertical vorticity for M3 (Fig 3) shows that the NOXP data collection region does include much of the stronger portion of the mesocyclone and its intensification.

### 2.2 NOXP Data

NOXP data, being X-band, need attenuation correction for reflectivity (Z) and differential reflectivity (Zdr). Such correction has been applied using techniques outlined in Schwarz and Burgess (2011; this conference). Please consult that paper for details. The NOXP data collection location (just north of Wewoka) is partially blocked by hills and trees when looking in the direction of the storm (north and northeast). Partial blockage extends to 3° elevation angle and is detrimental to observation of low-level features. When available returned signal maintains above threshold SNR, the quantities least affected by attenauation are radial velocity (V) and specific differential phase (Kdp). They are emphasized in low-level analysis. Examples of Z and V with partial beam blockage are seen in Fig 4.

The first NOXP volume scan (2334; all scans 1$^{o}$ to 7$^{o}$ in 1$^{o}$ steps every 2 min) depicts a broad hook echo (Fig 4) filled with precipitation. Also seen in the figure is the outline of a left-moving echo merging with the storm's right flank. The left-moving echo does not possess significant gradients in V and its merger does not seem to affect the structure or evolution of the storm.

Two vortex signatures are seen in radial velocity (Fig 4 right). The larger one corresponds to mesocyclone M2 and the smaller one appears to correspond to the Tecumseh/Seminole Airport tornado. Also shown on Fig 4 are results of the damage survey. The indicated EF2 damage (which ends by 2336) seems to best correlate with the tornado signature (which also ends by 2336). The broader area of EF0 damage (sometimes larger than 4 km in diameter) seems to best correlate with the mesocyclone signature. The reported damage continues to the northeast as the mesocyclone occludes, but retains strong low-level winds. As such, the latter part of the reported damage is believed to be mesocyclone wind damage. Maximum low-level ground-relative winds with the end of Tecumseh/Seminole Airport tornado at 2334 are 59 m/s. Maximum low-level ground-relative winds with M2 are 50 m/s at 2334 and slowly decrease to below 40 m/s near 2345, the reported time of the end of the damage path. A so-called Tornado Debris Signature (TDS; reduced Correlation Coefficient (Rhv) and reduced Zdr) is seen with the combination mesocyclone/tornado signature (see Schwarz and Burgess for an example). In this case, it appears mesocyclone winds are strong enough to lift light debris and produce a TDS.

## 3. DUAL-DOPPLER ANALYSIS

UMXP is operating by 2342 and dual-Doppler analysis begins. See Fig 4 for the location of UMXP and the baseline between NOXP and UMXP. Radial velocity , reflectivity, and Polarimetric variables are gridded using a multipass Barnes spatial interpolation scheme (Macjcen *et al* 2008), while wind synthesis follows the formulation of Ray *et al* (1980). The amount of partial beam blockage for NOXP and UMXP limit low-level data, requiring extrapolation of elevated data to the lowest level for use in calculations. This limits the accuracy of vertical velocity estimates (see Schwarz 2011 for more details and discussion of dual-Doppler set up and error sources).

Dual-Doppler wind synthesis at 2342 at 1 km overlaid on NOXP Z, Zdr, Rhv, and Kdp is seen in Fig 5. Note that the aforementioned partial beam blockage significantly affects the power-based variables (Z, Zdr, and Rhv) but not the phase-based variables (V and Kdp). By 2342, the occluding M2 is wrapped in heavy rain. A ribbon of updraft wraps back to and around M2 from the right flank WER where M3 is forming. Downdraft and southwesterly flow within and south of M2 have established a confluence zone with a pendant of rain along the right flank. This area marks the formation region of the new hook echo in association with M3. The downdraft that encompasses a large portion of M3 is very prominent at 3 km (Fig 6), and appears to be the same type of occlusion downdraft seen by Klemp and Rotunno (1983) and Wakimoto *et al* (1998). Note that confirmation of the downdraft is seen in the collocated reductions of Z, Zdr, and Kdp.

By 2346 (Fig 7), near the time of formation of the Clearview tornado, M3 has continued to strengthen at low levels and the pendant-hook echo/stretching-deformation zone have become more prominent. M2 continues to weaken and differential movement places it more and more to the rear of the echo.

An overall summary of low-level vertical vorticity (VVor) changes with time is presented in Fig 8. At 2342, M2 has large VVor (center to the northwest) although it has already begun to weaken and its center is already at a location well away from the favorable right storm flank. With time, M2 continues to weaken, and, as Fujita (1975) once remarked, "circulation is unhooking and going out of the back of the echo." M3, on the other hand (center to the southeast), is strengthening at low levels, and in conjunction with a pendant echo and a stretching/deformation zone, is in the process of producing a new, well-defined hook echo associated with increasing rotation. By 2348, VVor with M3 is approximately twice as strong as with M2, although 6 minutes earlier, the situation was reversed.

## 4. CONCLUDING REMARKS

A rather classic cyclic supercell occurs on May 10, 2010. Over its long life (>6 hours), it produces at least 11 mesocyclones and 20 tornadoes. Mesocyclone recurrence times vary from ~47 min early in storm life, to as little as ~17 min in middle storm life, and return to ~30 min in latter storm life. During the storm's life, several left-moving echoes merge with the storm right flank, but do not appear influence the strength or evolution of the storm.

VORTEX2 data is collected over only a small portion of the overall storm life. When mobile radar data collection (single-Doppler) begins, a mature mesocyclone (M2) and a tornado are occurring. M2 quickly begins to occlude and the tornado dissipates, but M2's low-level winds remain strong and continue producing wind damage for a period of time. The latter part of the damage path segment attributed to the tornado is likely instead produced by mesocyclone winds. Dual-Doppler wind synthesis reveals a strong occlusion downdraft associated with the weakening and eventual dissipation of M2.

M3 strengthens at low levels during the few minutes of dual-Doppler wind synthesis; a hook echo develops, wind speed and vorticity values increase, and a tornado forms. The evolution from a pendant echo with a developing stretching/deformation zone to a hook echo with a new mesocyclone along the stretching deformation zone compares favorably to the analysis of a cyclic supercell and a conceptual model of cyclic mesocyclogenesis presented by Beck *et al*, 2006.

Remaining work with the case will focus on trying to better understand tornadogenesis with M3. Unfortunately, limitations produced by 1) low-level partial beam blockage caused by intervening hills and trees, 2) low resolution resulting from increasing range from NOXP, and 3) only weak tornadogenesis observed until after the last dual-Doppler wind synthesis (not shown) all negatively affect tornadogenesis diagnosis. Trajectory analyses and calculation of forcing terms in the vorticity equation are underway, but ability to extract useful information is limited by the brief period of available 3D wind fields and the previously mentioned limitations.

## 5. ACKNOWLEDGMENTS

Funding was provided by NOAA/Office of Oceanic and Atmospheric Research under NOAA-University of Oklahoma Cooperative Agreement #NA17RJ1227, U.S. Department of Commerce. Funding was also provided by NSF Grant ATM-0802717and NSF Grant AGS-0821231. The three funding sources are greatly appreciated.

We would like to thank Josh Wurnan, VORTEX2 radar coordinator, who helped organize radar data collection, and the engineers and technicians under the leadership of Allen Zahrai who so ably maintain NOXP as a research instrument. We also would like to thank Ted Mansell, Blake Allen, and Valerie Melnikov for help with NOXP data collection and radar set up. We thank Vijay Venkatesh and Steve Frasier (U. Mass. MIRSL) for maintenance of UMXP and for data processing.

Nolan Atkins and his VORTEX2 crew, Kiel Ortega, and the OUN and TUL NWS Offices are thanked for help with the damage survey.

## 6. REFERENCES

Beck, J.R., J.L. Schroeder, and J. M. Wurman, 2006: High-resolution dual-Doppler analyses of the 29 May 2001 Kress, TX cyclic supercell. *Mon. Wea. Rev*, **134,** 3125-3148.

Burgess, D.W., R.J. Donaldson, Jr., and P.R. Derorchers, 1993: Tornado detection and warning by radar. Chapter 5 of **The Tornado: Its Structure, Dynamics, Prediction, and Hazards**, C Church, D. Burgess, B. Davies-Jones, C. Doswell (Ed), American Geophysical Union, Geophysical Monograph #79, Washington DC.

Fujita, T.T., 1975: New evidence form April 3-4,1974 tornadoes. *Preprints*, 9th Conf. Severe Local Storms, Norman, OK, Amer. Meteor. Soc., 248-255.

Klemp, J.B., and R. Rotunno, 1983: A study of the tornadic region within a supercell thunderstorm. *J. Atmos. Sci.*, **40**, 359-377.

Majcen, M., P. Markowski, Y. Richardson, D. Dowell, and J. Wurman, 2008: Mulitpass objective analysis of Doppler radar data. *J. Atmos. Ocean. Tech.*, **25**, 1845-1858.

Ray, P.S., C.L. Ziegler, W. Bumgarner, and R. Serafin, 1980: Single- and multi-Doppler radar observations of tornadic storms. *Mon. Wea. Rev.*, **108**, 1607-1625.

Schwarz, C.M., 2011: Supercell observations obtained during VORTEX2 from the NOAA (NSSL) X-band polarized mobile radar. M.S. Thesis. University of Oklahoma, 184 pp.

Schwarz, C.M. and D.W. Burgess, 2011: Supercell Polarimetric signatures at X-band: Data from VORTEX2. 35th Conf. on Radar Meteorology, Pittsburgh, PA, American Meteor. Soc., 26-30 October 2011, Poster Session 7.

Wakimoto, R.M., C. Liu, H. Cai, 1998: The Garden City, Kansas storm during VORTEX 95. Part I: Overview of the storm's life cycle and mesocyclogenesis. *Mon. Wea. Rev.*, **126**, 372-392.

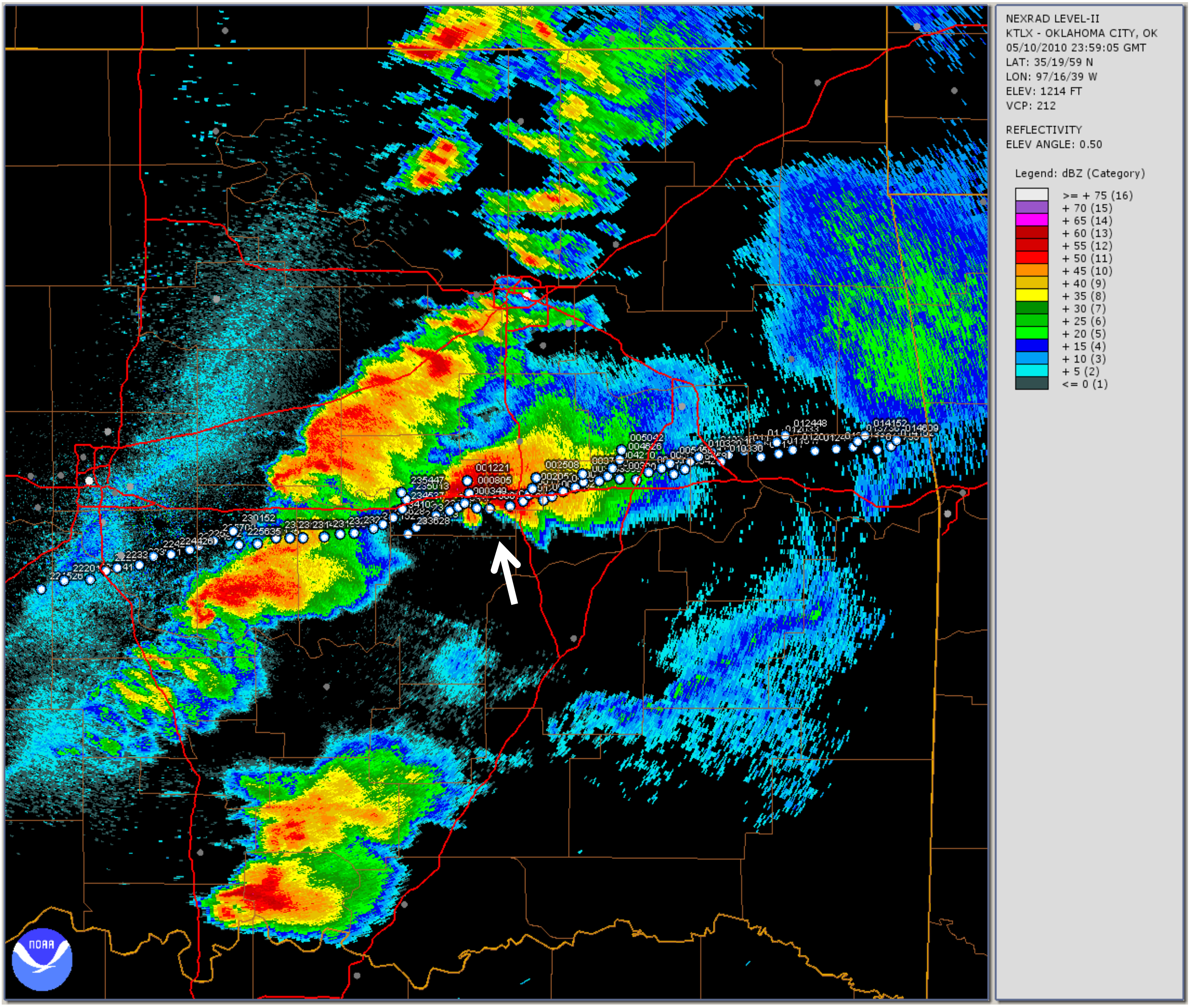


Figure 1. KTLX Level II radar image at 2359:05 UTC on 10 May 2010. Image produced by using NCDC Level II data viewer. Mesocyclone centers at ~ 1 km ARL height are marked with white dots. Location of the cyclic supercell at image time is indicated by the arrow.

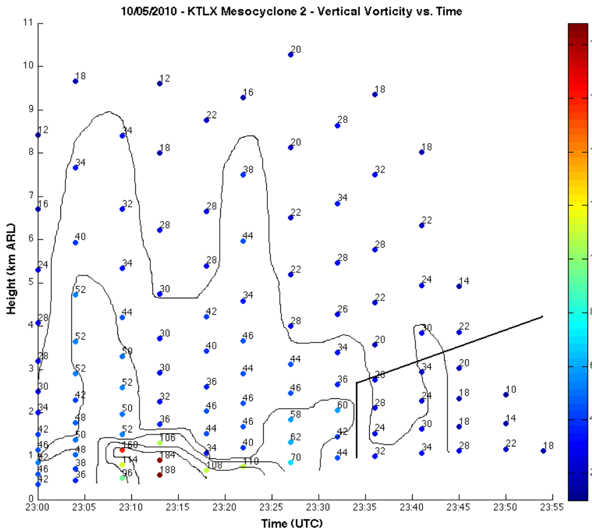


Figure 2. Time/height section of KTLX single-Doppler estimated Vertical Vorticity ($x10^{-3}$/s) for M2; contours begin with $30x10^{-3}$/s, and increasing in increments of $20x10^{-3}$/s. Dark lines mark region of VORTEX2 radar data collection.

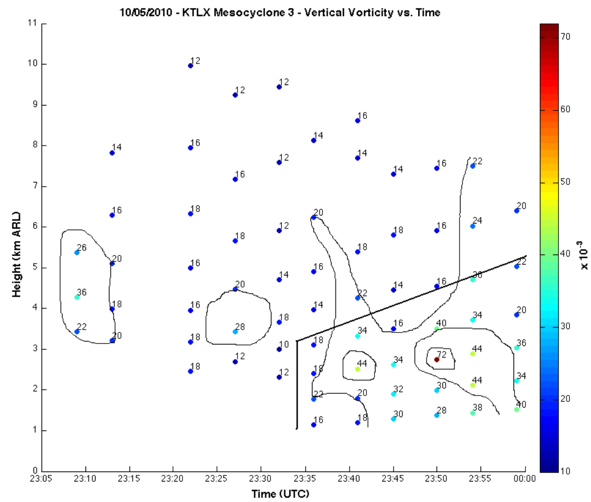


Figure 3. Same is Fig. 2 except beginning with $20x10^{-3}$/s.

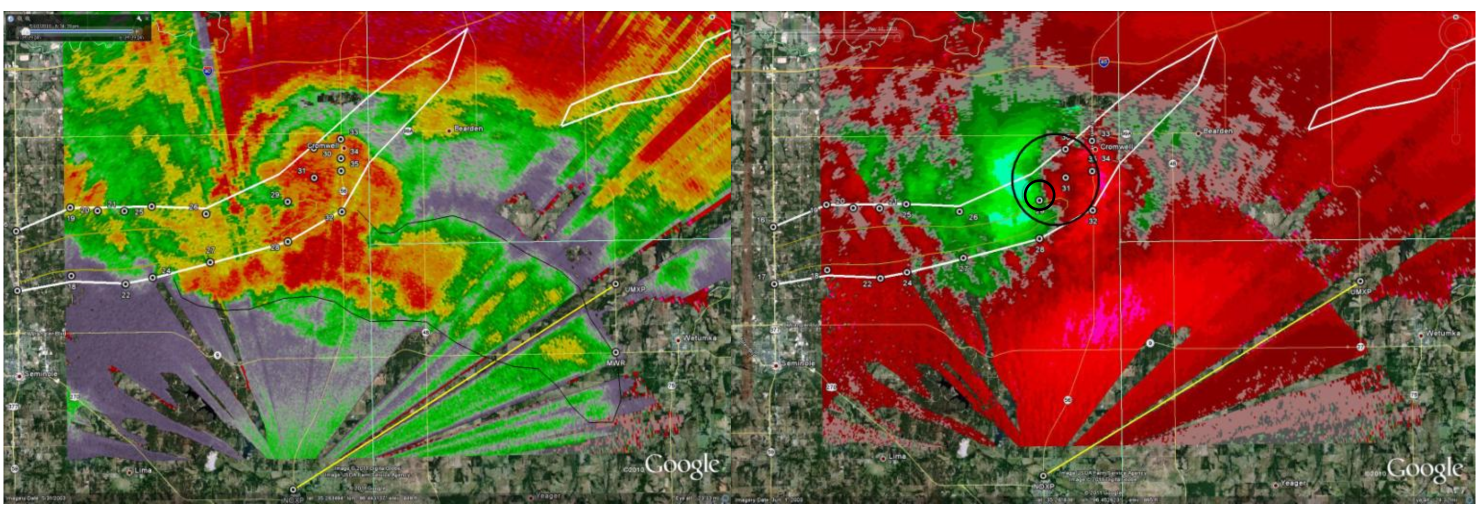

Figure 4. Google Earth images of attenuation-corrected reflectivity (left) and radial velocity (right) at 2334: 39 UTC, 3$^{o}$ elevation. White curve is outline of EF0 damage for Tecumseh/Seminole Airport tornado (left) and Clearview tornado (right); interior green curve marks EF2 damage for Tecumseh/Seminole Airport tornado. Black line (left panel) marks merging left-moving echo. Large dark circle (right) marks mesocyclone M2 signature, and small dark circle marks tornado signature. Long green line marks baseline between NOXP (lower left) and UMXP (upper right).

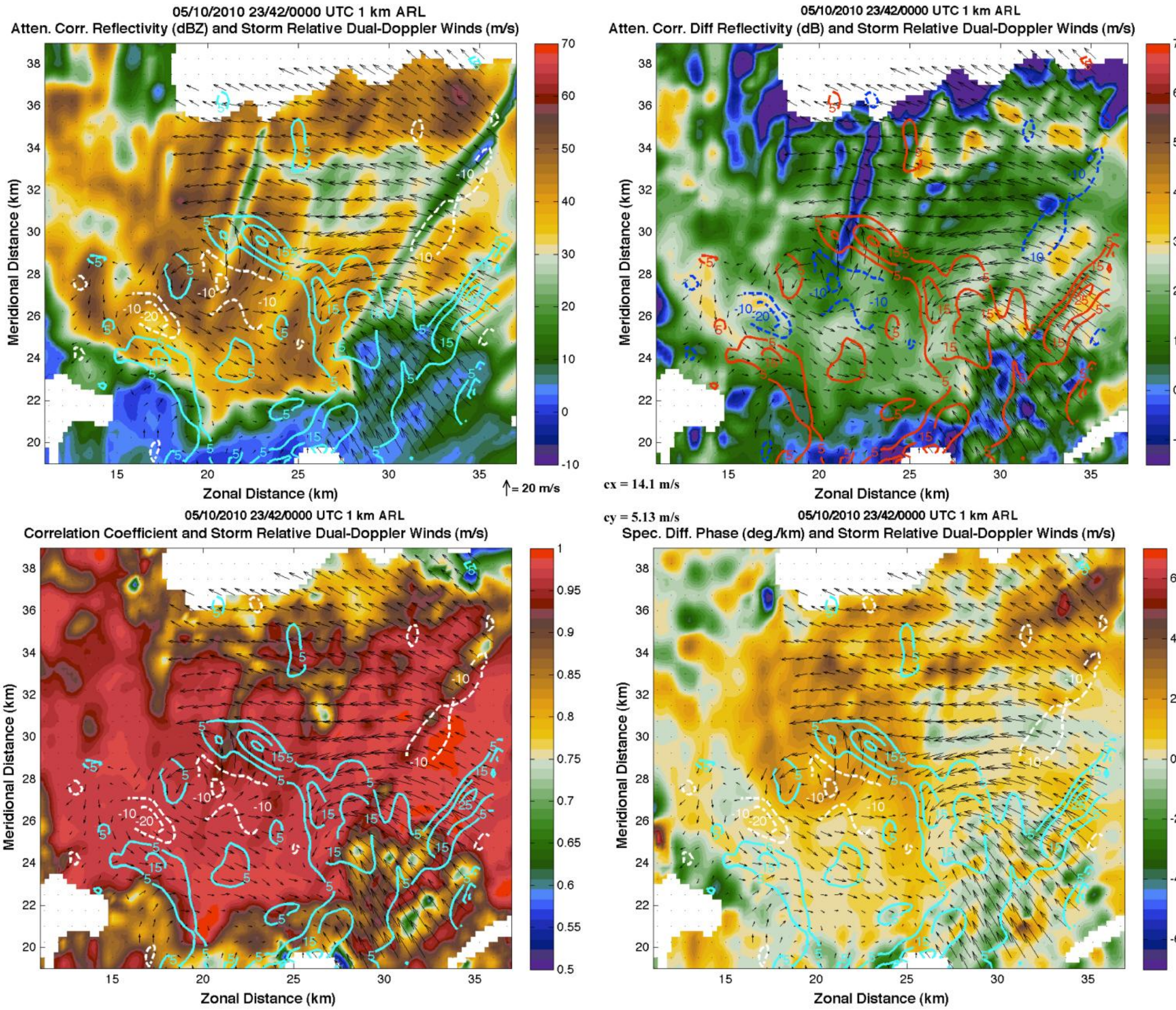


Figure 5. 4-panel of storm-relative dual-Doppler winds overlaid on attenuation-corrected Reflectivity (upper left), Differential Reflectivity (upper right), Correlation Coefficient (lower left), and Specific Differential Phase (lower right) for 2342 UTC at 1.5 km ARL. Solid (dashed) lines are upward (downward) vertical velocities.

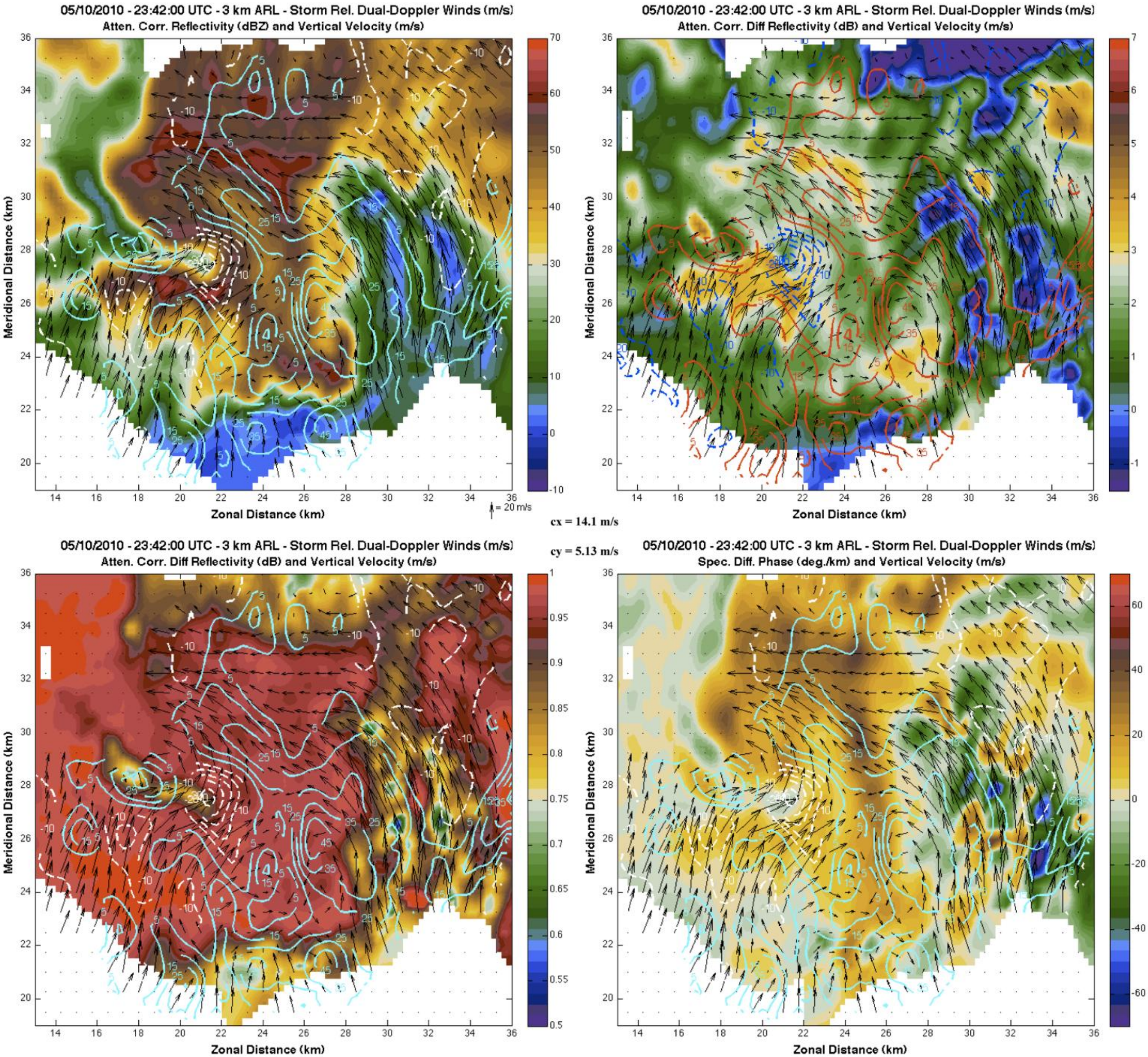


Figure 6. Same as Fig. 5 except at 3 km ARL.

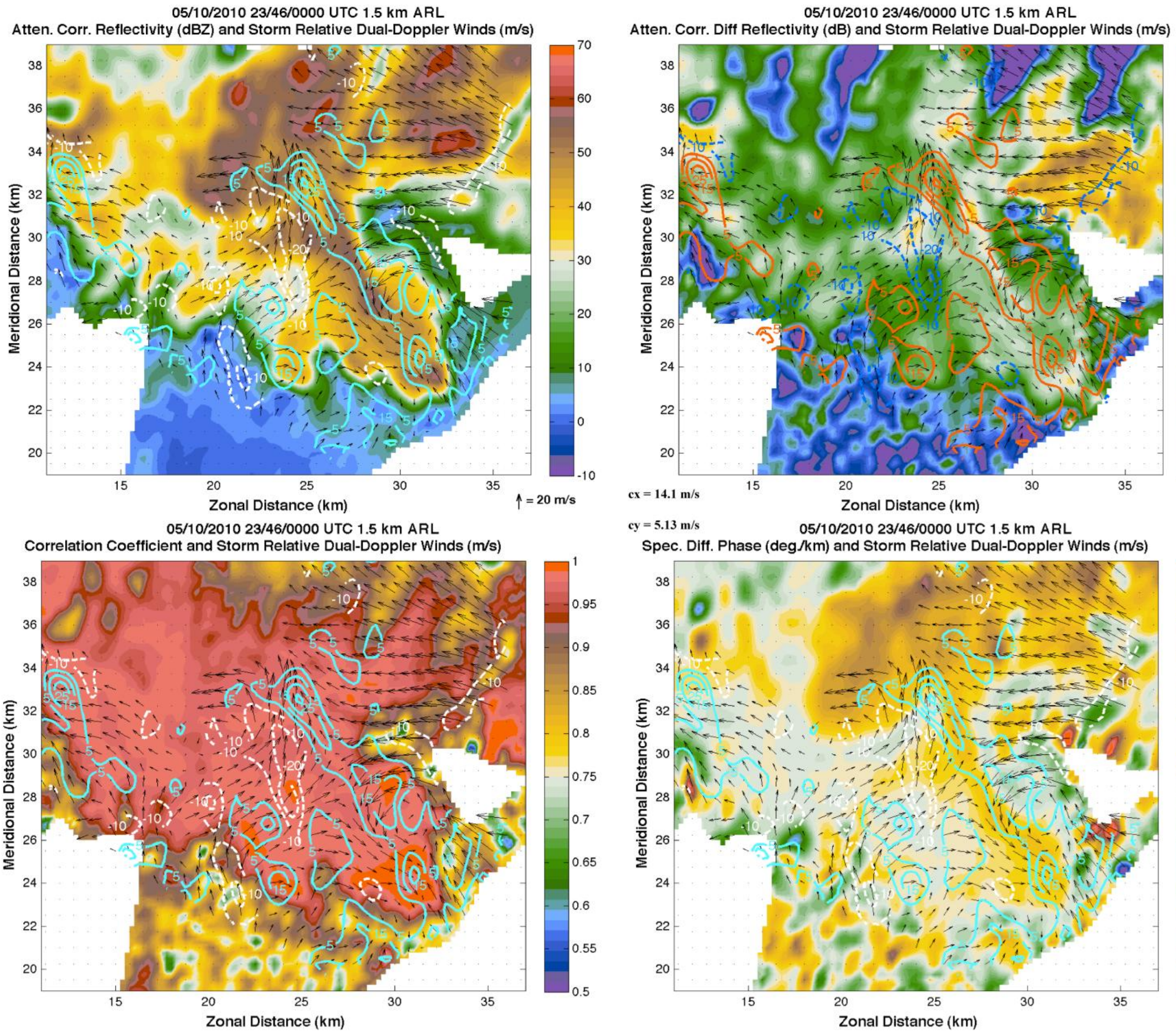


Figure 7. Same is Fig. 5 except at 2346 UTC at 1.5 km ARL.

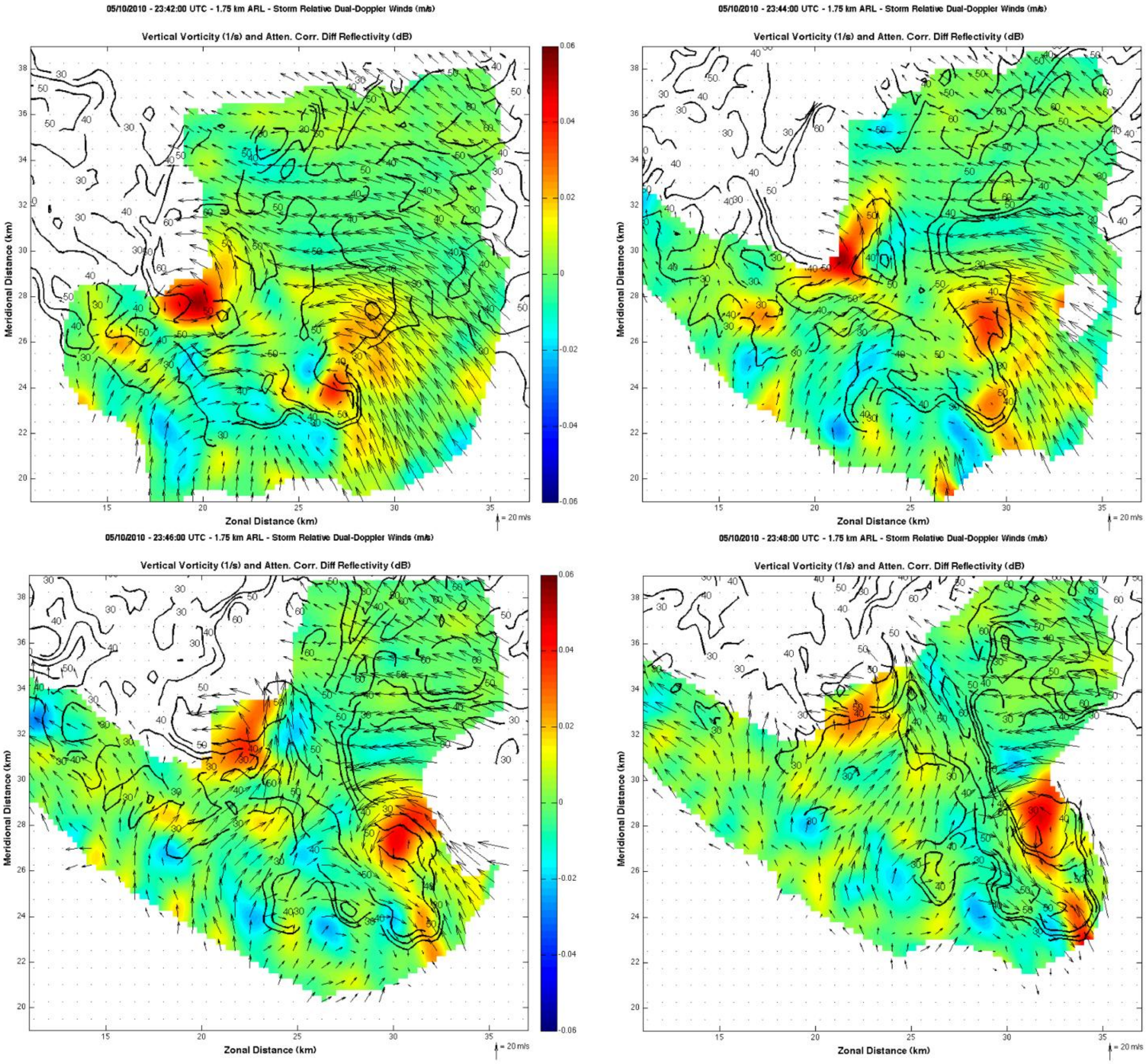


Figure 8. 4-panel of dual-Doppler wind vectors, vertical vorticity (color fill), reflectivity contours at 1.75 km ARL for 2342 UTC (upper left), 2344 UTC(upper right), 2346 UTC (lower left) and 2348 UTC (lower right).